

Voxel-MAE: Masked Autoencoders for Pre-training Large-scale Point Clouds

Chen Min^{1,2}, Dawei Zhao², Liang Xiao², Yiming Nie² and Bin Dai²

¹Peking University

²NIIDT

minchen@stu.pku.edu.cn

Abstract

Mask-based pre-training has achieved great success for self-supervised learning in image, video and language, without manually annotated supervision. However, as information redundant data, it has not yet been studied in the field of 3D object detection. As the point clouds in 3D object detection is large-scale, it is impossible to reconstruct the input point clouds. In this paper, we propose a mask voxel classification network for large-scale point clouds pre-training. Our key idea is to divide the point clouds into voxel representations and classify whether the voxel contains point clouds. This simple strategy makes the network to be voxel-aware of the object shape, thus improving the performance of 3D object detection. Extensive experiments show great effectiveness of our pre-trained model with 3D object detectors (SECOND, CenterPoint and PV-RCNN) on three popular datasets (KITTI, Waymo, and nuScenes). Codes are publicly available at <https://github.com/chaytonmin/Voxel-MAE>.

1. Introduction

3D object detection aims to obtain accurate 3D information by multiple sensors, which is one of the core techniques in autonomous driving. With the development of deep learning, many large-scale point clouds datasets [6, 21, 1] have been published and have greatly promoted the ability of environment perception for unmanned vehicles. However, the existing 3D object detection methods rely on large-scale annotated point clouds for model training. However, it needs to pay a lot of money and energy to collect and annotate the datasets. How to design the self-supervised learning task with the available large amount of unannotated point clouds to improve the performance of 3D object detectors has great significance to the perceptual ability of autonomous driving.

Self-supervised learning has been proven to be effective for learning representative features in computer vision [9, 23] and NLP [16, 24]. However, there is very lit-

tle research about self-supervised learning for large-scale point clouds. In particular, the simple masked autoencoders (MAE) have been proved effective in learning representative features with the masked data reconstruction task. Similar to 2D images and videos, the large-scale point clouds are also information redundant, thus designing the MAE for pre-training point clouds is also feasible. Unlike the 2D images or languages, the large amounts of point clouds in autonomous driving are hard to be reconstructed with neural networks.

In this paper, we focus on the voxel representation of large-scale point clouds. The voxel representation is widely used in 3D object detection [36, 28, 18]. The 3D Sparse Convolutions [28] with position encoding can focus on voxels with point clouds thus can reduce computation cost. The common voxel representation learning operators include mean operator, random sampling, and MLP operator [15]. Reconstructing the voxel features as a regression task is very difficult as the pre-training network needs to learn the distributions of each point. However, whether the voxel contains point clouds is more important to 3D object detectors. Thus, unlike the pixel reconstruction task in MAE for 2D images, we design the masked voxel classification task for large-scale point clouds, called Voxel-MAE, as illustrated in Fig. 1. That is, we first randomly mask some voxels, then put the masked voxels into the 3D autoencoder built by 3D sparse convolutions and the output of the 3D autoencoder is the probability of containing point clouds for each voxel, at last, we calculate the binary classification loss for the pretraining network. This masked voxel classification task pushes the encoder network to be voxel-aware to the whole shape of objects in point clouds, thus learning representative features for 3D object detection.

We validate the effectiveness of our Voxel-MAE with popular 3D object detectors, such as SECOND [28], CenterPoint [34] and PV-RCNN [18] on three widely used autonomous driving datasets, KITTI [6], Waymo [21] and nuScenes [1]. As large-scale point clouds in autonomous driving are information redundant data, Voxel-MAE with even a 90% masking ratio can still learn representative fea-

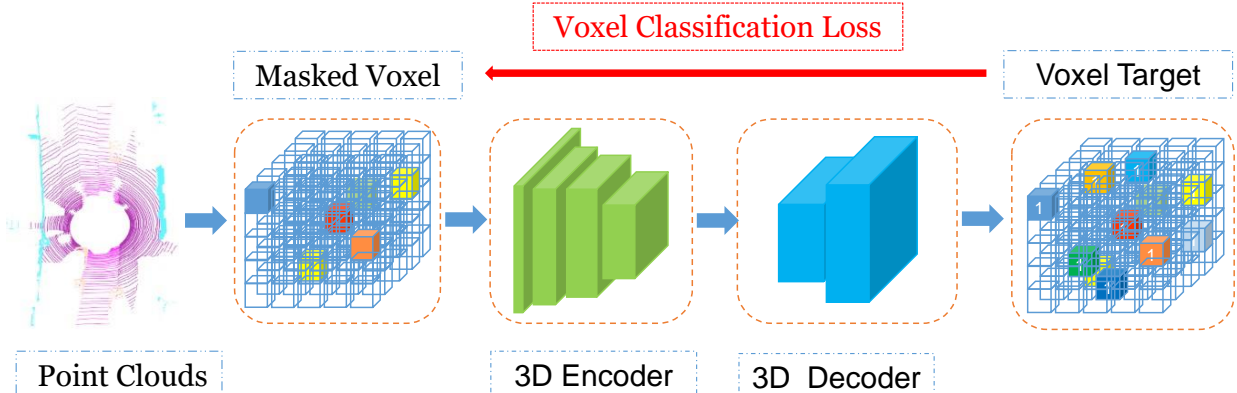


Figure 1. Overall architecture of our Voxel-MAE. We first divide the large-scale irregular point clouds into volumetric representations, and then randomly mask the voxels similar to MAE [9] and send the masked voxels to the asymmetric encoder-decoder network to reconstruct the voxels. Unlike MAE, the reconstruction target for large-scale point clouds is set to whether the voxel contains the point clouds. At last, the voxel binary classification loss is used to train the network end to end.

tures and improve the performance of 3D object detection. We also validate the effectiveness of Voxel-MAE in unsupervised domain adaptative 3D object detection, which proves the generalization ability of our Voxel-MAE in representation learning.

The main contributions of this work are listed below:

- We propose the simple but effective Voxel-MAE, with the novel masked voxel binary classification task, to learn representative features for pre-training large-scale point clouds.
- We validate the generalization ability of Voxel-MAE in unsupervised domain adaptive 3D object detection to address the domain shifts in LiDAR-based methods.
- We verify our Voxel-MAE on KITTI [6], Waymo [21], nuScenes [1] datasets with comprehensive experiments and effectively improves the performance of 3D object detection methods, such as SECOND [28], PV-RCNN [18] and CenterPoint [34].

2. Related Work

2.1. LiDAR-based 3D Object Detection

In recent years, learning-based 3D object detection methods have been tops in the challenge leaderboards of popular public datasets. Among them, LiDAR-based 3D object detection methods with the accurate 3D spatial information, have been widely used in the field of autonomous driving. Depending on the processing manner for point clouds, LiDAR-based 3D object detection methods can be categorized into point-based, voxel-based, and point-voxel-based.

Point-based object detectors, such as PointRCNN [19], 3DSSD [31] and Point-GNN [20], extract discriminative

features from raw point clouds with PointNet [13] and its improved version PointNet++ [14] and generate proposals centered at each point with 3D region proposal network. The drawback of point-based object detectors is the demand for the high computation cost. To address this problem, voxel-based detectors [36, 28, 11, 10, 33] transform the irregular point clouds into the volumetric representations. The pioneer VoxelNet [36] and its follower SECOND [28] apply the 3D CNNs and the Sparse 3D CNNs to regularize the 4D voxels. PointPillars[11] takes advantage of a standard 2D convolutional detection pipeline which codes point clouds into a special partition of voxels (i.e., pillars) in the light of the tradeoff between efficiency and accuracy. However, the step of point clouds discretization in voxel-based detectors will degrade the fine-grained localization accuracy [15]. Some point-voxel-based methods [18, 3, 32, 8] have been proposed, which take the advantage of localization accuracy of point-based detectors and computational efficiency of voxel-based detectors. PV-RCNN [18] first utilizes 3D sparse CNNs to encode the whole scene and then aggregates the multi-scale semantic voxel-wise features from 3D CNNs into keypoint features for localization refinement. How to design the pre-training network to improve the 3D detection performance has rarely been studied.

2.2. Domain Adaptive 3D Object Detection

Recently, some works that focus on addressing the domain shift on point clouds in the 3D object detection task have been proposed. SN [25] utilizes the target object size distribution prior to normalize the object from the source domain in order to close the size-level domain gap. The source-free domain adaptation method SF-UDA^{3D}[17], first scales the input target sequence data and re-scales the predictions, then uses the time consistency to score and refine the pseudo labels. SRDAN [35] adopts the scale-aware

Table 1. The details of our Voxel-MAE architecture which consists of Encoder and Decoder. 3DSparseCvconv and 3DTransCvconv denote 3D sparse convolution proposed in SECOND [28] and common 3D deconvolution respectively. Here we display the output size for pre-training SECOND on KITTI dataset.

Input	Layer Description	Output	Output Size
Input point clouds	Mean operator	Voxel representation	$1600 \times 1408 \times 41 \times 4$
Encoder			
Masked voxels \mathbf{V}_{input}	3DSparseCvconv, filter=(3,3,3), stride=(1,1,1)	Spconv_tensor_1	$1600 \times 1408 \times 41 \times 16$
Spconv_tensor_1	3DSparseCvconv, filter=(3,3,3), stride=(2,2,2)	Spconv_tensor_2	$800 \times 704 \times 21 \times 32$
Spconv_tensor_2	3DSparseCvconv, filter=(3,3,3), stride=(2,2,2)	Spconv_tensor_3	$400 \times 352 \times 11 \times 64$
Spconv_tensor_3	3DSparseCvconv, filter=(3,3,3), stride=(2,2,2)	Spconv_tensor_4	$200 \times 176 \times 5 \times 64$
Spconv_tensor_4	3DSparseCvconv, filter=(1,1,3), stride=(1,1,2)	Latent feature tensor	$200 \times 176 \times 2 \times 128$
Decoder			
Latent feature tensor	3DTransCvconv, filter=(3,3,3), stride=(2,2,2)	Dense_tensor_1	$400 \times 354 \times 4 \times 32$
Dense_tensor_1	3DTransCvconv, filter=(3,3,3), stride=(2,2,4)	Dense_tensor_2	$800 \times 704 \times 14 \times 8$
Dense_tensor_2	3DTransCvconv, filter=(3,3,3), stride=(2,2,3)	Occupancy voxels \mathbf{P}	$1600 \times 1408 \times 41 \times 1$

and range-aware feature adversarial alignment manners to match the distribution between source and target domain. MLC-Net [12] leverages the mean-teacher paradigm with three levels of consistency to facilitate the cross-domain transfer. The self-denoising frameworks, ST3D [30] and ST3D++ [29], employ three strategies (i.e., random object scaling, hybrid quality-aware triplet memory, and curriculum data augmentation), to reduce noise in pseudo label generation. Though achieving promising results, most of the aforementioned domain adaptation methods ignore the target data distribution when training the model with source data.

2.3. Self-supervised Learning

Self-supervised Learning (SSL) has been popular in recent years without the expensive data annotation. By designing pretext tasks, SSL can learn semantic representations and generalizes well in downstream tasks. [4] first proposes the pretext of predicting the relative location of image patches. [7, 27, 26] design the pretext task of rotation prediction that has shown promising results in representative feature learning. In [2], a jigsaw puzzle prediction task is proposed and generalizes well in domain adaptation object recognition. Although achieving remarkable progress, the above methods rely on the pretext task of data augmentation. Recently, MAE [9] first masks random patches of the input image and reconstructs the missing pixels with the simple autoencoder framework. VideoMAE [23] and [5] extend the MAE into spatiotemporal representation learning from videos that are more information redundant. In this paper, we explore the effectiveness of masked autoencoders in 3D object detection pre-training, as the point clouds are also information redundant.

3. Methodology

Inspired by the great self-supervised learning performance of MAE [9] in 2D images, we design the pretraining network of masked autoencoders for LiDAR-based 3D object detectors in order to learn representative features. With the n_s unlabeled point cloud data $\{\mathbf{X}^i\}_{i=1}^{n_s}$, we aim to first pre-train the masked autoencoders network ϕ_{pre} with only the point clouds data $\{\mathbf{X}^i\}_{i=1}^{n_s}$ to learn the high-level semantics. Then we use the pre-trained model ϕ_{pre} to warm up the 3D object detection network ϕ_s to improve the detection performance. The \mathbf{X}^i is the i -th source input point clouds. We also use the pre-trained network model ϕ_{pre} to domain adaptation task for the target point clouds $\{\mathbf{X}^j\}_{j=1}^{n_t}$. The proposed method is shown in Figure 1. We design the masked autoencoders for point clouds as the pretext task to warm up the 3D object detection network.

3.1. Masked Autoencoders

Given the instances from large-scale point clouds, the self-supervised pre-training task is to train the network with only the unlabeled data to generate good representations. How to design the proper pretext task is the main concern in self-supervised learning. The point clouds for 3D object detection in autonomous driving are huge and the masked reconstruction task is not suitable for large-scale point clouds. To mitigate the issue, we design the pretext task of masked voxel classification task for 3D object detection. We first randomly mask the voxels built from the input point clouds and then reconstruct the occupancy voxels with an autoencoder network. The pretext task is trained with the cross-entropy loss. The detailed architecture of Voxel-MAE is demonstrated in Table 1.

3.1.1 Masking

Following the common setting in 3D point cloud detection, the point clouds are divided into equally spaced voxels. For the point cloud with range $W \times H \times D$ along the $X \times Y \times Z$ respectively, the size of a voxel is $v_W \times v_H \times v_D$ accordingly. The total number of voxels that contains point clouds is n_v . Following the 3D object detector benchmark SECOND [28], we directly calculate the mean of point features with the 3D coordinates and reflectance intensities in a certain voxel as the voxel-wise representation.

As the large-scale point clouds are information-redundant, we take the random masking strategy with the masking ratio r on all the voxels, which is agnostic to the 3D spatial structure of large-scale point clouds, thus the set of voxels $\mathbf{V}_{input} \in R^{n_v \times r \times 4}$ are used as the training set. The occupancy voxels containing point clouds $\mathbf{T} \in R^{n_v \times 1}$ (the value of each voxel is 1) is used as ground truth for voxel classification loss.

3.1.2 Encoder

As the number of point clouds is very large, the Transformer network used in MAE [9] is not suitable for our case. We adopt the 3D sparse convolution [28] to build the encoder network, in which position encoding is applied to contain the positional information and improve training efficiency. As the 3D sparse convolution only focuses on the voxels containing point clouds, our voxel masking strategy can reduce the memory complexity for training, similar to Transformer network.

3.1.3 Decoder

Our decoder consists of several 3D convolution layers and the last layer outputs the probability of each voxel containing point clouds. The output of decoder is $\mathbf{P} \in R^{n_v \times 1}$. The decoder is only used during pre-training to perform voxel classification task, similar to MAE. Shifting mask tokens to the decoder can make the encoder learn better latent features for 3D object detection.

3.1.4 Reconstruction Target

We use the 3D convolution layer as the prediction head to produce the reconstructed occupancy voxels. The aim is to recover the coordinates of voxels in the masked set. Given the predicted occupancy voxels \mathbf{P} and ground truth occupancy voxels \mathbf{T} , we calculate the binary voxel classification loss of cross-entropy:

$$loss = -\frac{1}{batch} \sum_{i=0}^{batch} \sum_{j=1}^{n_v} \mathbf{T}_j^i \log \mathbf{P}_j^i, \quad (1)$$

Table 2. Performance comparison on the KITTI *val* split with AP calculated by 11 recall positions.

Methods	Car	Pedestrian	Cyclist
SECOND [28]	78.62	52.98	67.15
SECOND+ours	78.89	53.32	68.00
SECOND-IOU [30]	79.09	55.74	71.31
SECOND-IOU+ours	79.21	55.82	72.18
PV-RCNN [18]	83.61	57.90	70.47
PV-RCNN+ours	83.75	59.36	71.99

where \mathbf{P}_j^i is the predicted probability of voxel j of the i -th training sample, and \mathbf{T}_j^i is the corresponding ground truth.

Albeit simple, the masked voxel classification loss effectively introduces the information of point cloud non-uniform distribution to facilitate the object detectors to learn representative features.

4. Experiments

4.1. Experimental Setup

Dataset The three popular autonomous driving datasets: KITTI [6], Waymo [21] and nuScenes [1] are used in our experiments.

KITTI. The KITTI dataset [6] is one of the most popular autonomous driving datasets, which provides 7,481 training samples and 7,518 testing samples. The 3D bounding box annotations are only provided within the Field of View (FoV) of the front camera. We follow the common 50/50 *train/val* split and use the official KITTI evaluation metrics for three-level evaluation (Easy, Moderate, Hard) and the mean average precision is evaluated.

Waymo Open Dataset. The Waymo Open Dataset [21] is a recently released large-scale autonomous driving dataset, which consists of total 798 training sequences with around 158,361 LiDAR samples, and 202 validation sequences with 40,077 LiDAR samples. Following the popular point cloud detection codebase OpenPCDet [22], we subsample a single frame of 20% data (about 32k frames) of all the training samples as the training set. It annotated the objects in the full 360° field. The official evaluation metrics of Waymo are mean average precision (AP) and mean average precision weighted by heading (APH) in difficulty levels (L1 and L2).

nuScenes. The nuScenes dataset [1] is another popular autonomous driving dataset. There are total 28,130 training samples and 6,019 validation samples. We evaluate with the official evaluation metrics of the nuScenes Detection Score (NDS), mean average precision (mAP), average translation error (ATE), average scale error (ASE), average orientation error (AOE), average velocity error (AVE), average attribute error (AAE).

Table 3. Performance comparison on the KITTI *val* split with AP calculated by 11 recall positions on evaluation of bounding box and orientation.

Evaluation	Method	Car			Pedestrain			Cyclist		
		Easy	Moderate	Hard	Easy	Moderate	Hard	Easy	Moderate	Hard
bbox	SECOND [28]	90.73	89.76	88.94	68.70	65.27	62.52	87.88	75.43	71.67
	SECOND+ours	94.78	89.99	89.15	70.36	67.36	65.04	91.78	78.68	73.86
aos	SECOND [28]	90.73	89.63	88.70	63.46	60.13	56.93	87.63	74.67	71.00
	SECOND+ours	94.77	89.89	88.96	65.29	61.65	59.11	91.63	78.34	73.46

Table 4. Quantitative detection performance achieved by different methods on the Waymo validation set.

Methods	Vec_L1		Vec_L2		Ped_L1		Ped_L2		Cyc_L1		Cyc_L2	
	mAP	mAPH										
SECOND [28]	70.96	70.34	62.58	62.02	65.23	54.24	57.22	47.49	57.13	55.62	54.97	53.53
SECOND+ours	71.18	70.56	62.88	62.31	67.19	55.61	59.05	48.77	57.71	56.21	55.58	54.13
CenterPoint [34]	71.33	70.76	63.16	62.65	72.09	65.49	64.27	58.23	68.68	67.39	66.11	64.87
CenterPoint+ours	71.87	71.31	64.03	63.51	73.90	67.10	65.80	59.61	70.28	69.02	67.75	66.52
PV-RCNN(Anchor) [18]	75.41	74.74	67.44	66.80	71.98	61.24	63.70	53.95	65.88	64.25	63.39	61.82
PV-RCNN(Anchor)+ours	76.25	75.32	68.34	67.15	72.92	62.32	64.14	54.25	66.73	65.39	64.23	62.66
PV-RCNN(Center) [22]	75.95	75.43	68.02	67.54	75.94	69.40	67.66	61.62	70.18	68.98	67.73	66.57
PV-RCNN(Center)+ours	77.34	76.82	68.70	68.23	77.70	71.15	69.54	63.45	70.54	69.39	68.10	66.99

Implementation Details We adopt the training settings of the popular point cloud detection codebase OpenPCDet [22] (version 0.5.2). For KITTI dataset, the detection range is set to [0, 70.4m] for X axes, [-40m, 40m] for Y axes, [-3m, 1m] for Z axes, and the voxel size is set to (0.05m, 0.05m, 0.1m). For Waymo dataset, the detection range is set to [-75.2m, 75.2m] for X and Y axes, [-2m, 4m] for Z axes, and the voxel size is set to (0.1m, 0.1m, 0.15m). For nuScenes dataset, the detection range is set to [-51.2m, 51.2m] for X and Y axes, [-5m, 3m] for Z axes, and the voxel size is set to (0.1m, 0.1m, 0.2m).

Following OpenPCDet, we use the common augmentations, including random world flipping and random world scaling in training Voxel-MAE. The ADAM optimizer and cosine annealing learning rate strategy are adopted. More detailed parameter setups could be found in OpenPCDet.

4.2. Results and Analysis

Table 2 shows the performance of the proposed pre-training network Voxel-MAE on KITTI val set. Although the number of samples in KITTI is small, our Voxel-MAE can still improve the SECOND and PVRCNN, especially for the small objects (i.e., pedestrian and cyclist). We also find that our Voxel-MAE can improve the evaluation of the bounding box and orientation a lot, as shown in Table 3. This is because our voxel masking strategy can help to learn high-level semantic information as the Voxel-MAE needs to recover these totally missing voxels. The bounding box and orientation predicting will benefit from such a design.

To further validate the effectiveness of our proposed Voxel-MAE, we evaluate the performance of Voxel-MAE on the large-scale Waymo and nuScenes datasets. Table 4

shows that our method improves the popular 3D point cloud detection methods SECOND, Centerpoint, and PV-RCNN in terms of mAP and mAPH. The experimental results on the large-scale Waymo and nuScenes dataset further validate the great representative features obtained by our simple Voxel-MAE on various datasets.

4.3. Unsupervised Domain Adaptation

The domain shifts in LiDAR-based 3D objectors are obvious as the LiDARs have different scan patterns. Evaluation of datasets captured in different locations, conditions, or sensors than that of the training (source) data results in a drop in model performance due to the gap in distribution with the test (or target) data. To further investigate the generalization ability of Voxel-MAE in representation learning, we conduct experiments in two scenarios of unsupervised domain adaptive (UDA) 3D object detection: different data collection locations and time (i.e., Waymo → KITTI) and different LiDAR ring numbers (i.e., nuScenes → KITTI). We compare our method with (1) Oracle, where the model training and evaluation are both on the target domain; (2) Soure-only, where the pre-trained model is directly used on the target domain inferring; (3) SN [25], a weakly-supervised domain adaptation method with the statistical information of target domain object size; (4) ST3D [30]; the SOTA UDA 3D object detection method with self-training strategy and (5) ST3D(w/SN) [30], where the weakly-supervised DA setting utilizes the target object size distribution as prior; the SOTA UDA 3D object detection method with self-training strategy. We follow the setting in the recently published UDA method ST3D [30] and use the pre-trained model by our Voxel-MAE to train ST3D.

Table 5. Quantitative detection performance achieved by different methods on the nuScenes validation set.

Methods	mAP	NDS	mATE	mASE	mAOE	mAVE	mAAE
SECOND [28]	50.59	62.29	31.15	25.51	26.64	26.26	20.46
SECOND+ours	51.32	63.24	31.32	26.24	27.37	27.54	21.33
Centerpoint [34]	56.03	64.54	30.11	25.55	38.28	21.94	18.87
Centerpoint+ours	57.25	65.23	31.45	25.63	39.22	22.12	20.14

Table 6. Quantitative results of adaptation tasks. Our Voxel-MAE can improve the performance of unsupervised domain adaptation.

Task	Method	PV-RCNN	
		BEV	3D
Waymo → KITTI	Oracle	88.98	82.50
	Source-only	61.18	22.01
	SN [25]	79.78	63.60
	ST3D [30]	84.10	64.78
	ST3D(w/SN) [30]	86.65	76.86
	ST3D+Ours	85.52	65.24
nuScenes → KITTI	ST3D(w/SN)+Ours	87.15	77.13
	Oracle	88.98	82.50
	Source-only	68.15	37.17
	SN [25]	60.48	49.47
	ST3D [30]	78.36	70.85
	ST3D(w/SN) [30]	84.29	72.94
	ST3D+Ours	78.66	71.24
	ST3D(w/SN)+Ours	85.43	73.22

From Table 6, we can see that with our Voxel-MAE, the performance of UDA is improved, which demonstrates that our Voxel-MAE can learn more transferable representations.

4.4. Ablation Studies

In this section, we conduct extensive ablation experiments to investigate the individual components of our Voxel-MAE. All experiments are conducted with the 3D detector SECOND [28] on KITTI *val* split.

4.4.1 Pretext Task

We now analyze the influence of the reconstruction task of Voxel-MAE. In Table 7 we can observe that the results of the voxel regression task will decrease. This may be because the voxel classification task is easier for the network to learn and whether the voxel contains point clouds is more important for voxel-based 3D object detection methods. With the simple voxel binary classification task, the pre-trained network would be voxel-aware of object shape, thus improving the performance of the downstream task. The results in Table 7 are achieved by 11 recall positions on evaluation of 3d detection on three categories.

Table 7. Impacts of pretext task.

Target	Car	Pedestrian	Cyclist
Regression	78.39	52.75	67.32
Classification	78.89	53.32	68.00

Table 8. Impacts of masking ratio.

Ratio	Easy	Moderate	Hard
0.3	96.96	94.75	93.97
0.5	97.03	94.79	94.00
0.7	97.14	94.78	94.11
0.9	97.00	96.06	94.13

Table 9. Impacts of pre-training times.

Epoch	Easy	Moderate	Hard
1	78.98	66.13	61.55
5	80.46	66.18	62.79
10	82.16	68.00	62.56
15	81.63	67.35	61.93

4.4.2 Masking Ratio

In this section, we study the effect of the voxel masking ratio on the pre-training input. It can be seen from Table 8 that an extremely high masking ratio (90%) can still achieve good representations. We choose the masking ratio of 50% for the experiments on three datasets for simplicity. The results in Table 8 are achieved by 40 recall positions on evaluation of 3d detection on car category with IOU threshold 0.5.

4.4.3 Pre-training Times

Table 9 shows the influence of the training times. The results are achieved by 11 recall positions on evaluation of 3d detection on cyclist category with IOU threshold 0.5. With the increment of training times, the performance increases at first and afterward decreases. The number of pre-training epochs for KITTI, Waymo, and nuScenes set as 10, 15, and 10, respectively.

5. Conclusion

In this paper, we introduce a simple large-scale point clouds self-supervised learning method, named Voxel-MAE, for 3D object detection pre-training. Our Voxel-MAE first randomly masks the input voxels and then recon-

structs the voxels. Different from 2D MAE, we design the voxel classification task for large-scale point clouds, which would encourage the Voxel-MAE to reason over high-level semantics to recover these masked voxels, because whether the voxel contains point clouds is very important for 3D object detection. Our extensive experimental results demonstrate the effectiveness of Voxel-MAE on three popular autonomous driving datasets, KITTI, Waymo, and nuScenes. In the future, we are planning to validate the effectiveness of Voxel-MAE in more downstream tasks for large-scale point clouds.

References

- [1] Holger Caesar, Varun Bankiti, Alex H Lang, Sourabh Vora, Venice Erin Liang, Qiang Xu, Anush Krishnan, Yu Pan, Giacarlo Baldan, and Oscar Beijbom. nuscenes: A multi-modal dataset for autonomous driving. In *Proceedings of the IEEE/CVF conference on computer vision and pattern recognition*, pages 11621–11631, 2020. [1](#), [2](#), [4](#)
- [2] Fabio M Carlucci, Antonio D’Innocente, Silvia Bucci, Barbara Caputo, and Tatiana Tommasi. Domain generalization by solving jigsaw puzzles. In *Proceedings of the IEEE/CVF Conference on Computer Vision and Pattern Recognition*, pages 2229–2238, 2019. [3](#)
- [3] Yilun Chen, Shu Liu, Xiaoyong Shen, and Jiaya Jia. Fast point r-cnn. In *Proceedings of the IEEE/CVF international conference on computer vision*, pages 9775–9784, 2019. [2](#)
- [4] Carl Doersch, Abhinav Gupta, and Alexei A Efros. Unsupervised visual representation learning by context prediction. In *Proceedings of the IEEE international conference on computer vision*, pages 1422–1430, 2015. [3](#)
- [5] Christoph Feichtenhofer, Haoqi Fan, Yanghao Li, and Kaiming He. Masked autoencoders as spatiotemporal learners. *arXiv preprint arXiv:2205.09113*, 2022. [3](#)
- [6] Andreas Geiger, Philip Lenz, and Raquel Urtasun. Are we ready for autonomous driving? the kitti vision benchmark suite. In *2012 IEEE conference on computer vision and pattern recognition*, pages 3354–3361. IEEE, 2012. [1](#), [2](#), [4](#)
- [7] Spyros Gidaris, Praveer Singh, and Nikos Komodakis. Unsupervised representation learning by predicting image rotations. *arXiv preprint arXiv:1803.07728*, 2018. [3](#)
- [8] Chenhang He, Hui Zeng, Jianqiang Huang, Xian-Sheng Hua, and Lei Zhang. Structure aware single-stage 3d object detection from point cloud. In *Proceedings of the IEEE/CVF conference on computer vision and pattern recognition*, pages 11873–11882, 2020. [2](#)
- [9] Kaiming He, Xinlei Chen, Saining Xie, Yanghao Li, Piotr Dollár, and Ross Girshick. Masked autoencoders are scalable vision learners. In *Proceedings of the IEEE/CVF Conference on Computer Vision and Pattern Recognition*, pages 16000–16009, 2022. [1](#), [2](#), [3](#), [4](#)
- [10] Hongwu Kuang, Bei Wang, Jianping An, Ming Zhang, and Zehan Zhang. Voxel-fpn: Multi-scale voxel feature aggregation for 3d object detection from lidar point clouds. *Sensors*, 20(3):704, 2020. [2](#)
- [11] Alex H Lang, Sourabh Vora, Holger Caesar, Lubing Zhou, Jiong Yang, and Oscar Beijbom. Pointpillars: Fast encoders for object detection from point clouds. In *Proceedings of the IEEE/CVF conference on computer vision and pattern recognition*, pages 12697–12705, 2019. [2](#)
- [12] Zhipeng Luo, Zhongang Cai, Changqing Zhou, Gongjie Zhang, Haiyu Zhao, Shuai Yi, Shijian Lu, Hongsheng Li, Shanghang Zhang, and Ziwei Liu. Unsupervised domain adaptive 3d detection with multi-level consistency. In *Proceedings of the IEEE/CVF International Conference on Computer Vision*, pages 8866–8875, 2021. [3](#)
- [13] Charles R Qi, Hao Su, Kaichun Mo, and Leonidas J Guibas. Pointnet: Deep learning on point sets for 3d classification and segmentation. In *Proceedings of the IEEE conference on computer vision and pattern recognition*, pages 652–660, 2017. [2](#)
- [14] Charles Ruizhongtai Qi, Li Yi, Hao Su, and Leonidas J Guibas. Pointnet++: Deep hierarchical feature learning on point sets in a metric space. *Advances in neural information processing systems*, 30, 2017. [2](#)
- [15] Rui Qian, Xin Lai, and Xirong Li. 3d object detection for autonomous driving: a survey. *Pattern Recognition*, page 108796, 2022. [1](#), [2](#)
- [16] Alec Radford, Karthik Narasimhan, Tim Salimans, Ilya Sutskever, et al. Improving language understanding by generative pre-training. 2018. [1](#)
- [17] Cristiano Saltori, Stéphane Lathuilière, Nicu Sebe, Elisa Ricci, and Fabio Galasso. Sf-uda 3d: Source-free unsupervised domain adaptation for lidar-based 3d object detection. In *2020 International Conference on 3D Vision (3DV)*, pages 771–780. IEEE, 2020. [2](#)
- [18] Shaoshuai Shi, Chaoxu Guo, Li Jiang, Zhe Wang, Jianping Shi, Xiaogang Wang, and Hongsheng Li. Pv-rnn: Point-voxel feature set abstraction for 3d object detection. In *Proceedings of the IEEE/CVF Conference on Computer Vision and Pattern Recognition*, pages 10529–10538, 2020. [1](#), [2](#), [4](#), [5](#)
- [19] Shaoshuai Shi, Xiaogang Wang, and Hongsheng Li. Pointrcnn: 3d object proposal generation and detection from point cloud. In *Proceedings of the IEEE/CVF conference on computer vision and pattern recognition*, pages 770–779, 2019. [2](#)
- [20] Weijing Shi and Raj Rajkumar. Point-gnn: Graph neural network for 3d object detection in a point cloud. In *Proceedings of the IEEE/CVF conference on computer vision and pattern recognition*, pages 1711–1719, 2020. [2](#)
- [21] Pei Sun, Henrik Kretzschmar, Xerxes Dotiwalla, Aurelien Chouard, Vijaysai Patnaik, Paul Tsui, James Guo, Yin Zhou, Yuning Chai, Benjamin Caine, et al. Scalability in perception for autonomous driving: Waymo open dataset. In *Proceedings of the IEEE/CVF conference on computer vision and pattern recognition*, pages 2446–2454, 2020. [1](#), [2](#), [4](#)
- [22] OpenPCDet Development Team. Openpcdet: An open-source toolbox for 3d object detection from point clouds. <https://github.com/open-mmlab/OpenPCDet>, 2020. [4](#), [5](#)
- [23] Zhan Tong, Yibing Song, Jue Wang, and Limin Wang. Videomae: Masked autoencoders are data-efficient learn-

ers for self-supervised video pre-training. *arXiv preprint arXiv:2203.12602*, 2022. 1, 3

[24] Ashish Vaswani, Noam Shazeer, Niki Parmar, Jakob Uszkoreit, Llion Jones, Aidan N Gomez, Łukasz Kaiser, and Illia Polosukhin. Attention is all you need. *Advances in neural information processing systems*, 30, 2017. 1

[25] Yan Wang, Xiangyu Chen, Yurong You, Li Erran Li, Bharath Hariharan, Mark Campbell, Kilian Q Weinberger, and Wei-Lun Chao. Train in germany, test in the usa: Making 3d object detectors generalize. In *Proceedings of the IEEE/CVF Conference on Computer Vision and Pattern Recognition*, pages 11713–11723, 2020. 2, 5, 6

[26] Liang Xiao, Jiaolong Xu, Dawei Zhao, Zhiyu Wang, Li Wang, Yiming Nie, and Bin Dai. Self-supervised domain adaptation with consistency training. In *2020 25th International Conference on Pattern Recognition (ICPR)*, pages 6874–6880. IEEE, 2021. 3

[27] Jiaolong Xu, Liang Xiao, and Antonio M López. Self-supervised domain adaptation for computer vision tasks. *IEEE Access*, 7:156694–156706, 2019. 3

[28] Yan Yan, Yuxing Mao, and Bo Li. Second: Sparsely embedded convolutional detection. *Sensors*, 18(10):3337, 2018. 1, 2, 3, 4, 5, 6

[29] Jihan Yang, Shaoshuai Shi, Zhe Wang, Hongsheng Li, and Xiaojuan Qi. St3d++: Denoised self-training for unsupervised domain adaptation on 3d object detection. *arXiv preprint arXiv:2108.06682*, 2021. 3

[30] Jihan Yang, Shaoshuai Shi, Zhe Wang, Hongsheng Li, and Xiaojuan Qi. St3d: Self-training for unsupervised domain adaptation on 3d object detection. In *Proceedings of the IEEE/CVF Conference on Computer Vision and Pattern Recognition*, pages 10368–10378, 2021. 3, 4, 5, 6

[31] Zetong Yang, Yanan Sun, Shu Liu, and Jiaya Jia. 3dssd: Point-based 3d single stage object detector. In *Proceedings of the IEEE/CVF conference on computer vision and pattern recognition*, pages 11040–11048, 2020. 2

[32] Zetong Yang, Yanan Sun, Shu Liu, Xiaoyong Shen, and Jiaya Jia. Std: Sparse-to-dense 3d object detector for point cloud. In *Proceedings of the IEEE/CVF international conference on computer vision*, pages 1951–1960, 2019. 2

[33] Maosheng Ye, Shuangjie Xu, and Tongyi Cao. Hvnet: Hybrid voxel network for lidar based 3d object detection. In *Proceedings of the IEEE/CVF conference on computer vision and pattern recognition*, pages 1631–1640, 2020. 2

[34] Tianwei Yin, Xingyi Zhou, and Philipp Krahenbuhl. Center-based 3d object detection and tracking. In *Proceedings of the IEEE/CVF conference on computer vision and pattern recognition*, pages 11784–11793, 2021. 1, 2, 5, 6

[35] Weichen Zhang, Wen Li, and Dong Xu. Srdan: Scale-aware and range-aware domain adaptation network for cross-dataset 3d object detection. In *Proceedings of the IEEE/CVF Conference on Computer Vision and Pattern Recognition*, pages 6769–6779, 2021. 2

[36] Yin Zhou and Oncel Tuzel. Voxelnet: End-to-end learning for point cloud based 3d object detection. In *Proceedings of the IEEE conference on computer vision and pattern recognition*, pages 4490–4499, 2018. 1, 2